HHS Public Access

Author manuscript

*J Phys Chem Lett*. Author manuscript; available in PMC 2020 October 17.

Published in final edited form as:

*J Phys Chem Lett*. 2019 October 17; 10(20): 6293–6300. doi:10.1021/acs.jpclett.9b02291.

# Multi-State Multi-Configuration Quantum Chemical Computation of the Two-Photon Absorption Spectra of Bovine Rhodopsin

**Samira Gholami**[a], **Laura Pedraza-González**[b], **Xuchun Yang**[a], **Alexander. A. Granovsky**[c], **Ilya. N. Ioffe**[d], **Massimo Olivucci**[a,b]

[a]Department of Chemistry, Bowling Green State University, Bowling Green, Ohio 43403, United States

[b]Department of Biotechnology, Chemistry and Pharmacy, Università di Siena, via A. Moro 2, I-53100 Siena, Siena, Italy

[c]Firefly Project, Moscow 117593, Russia

[d]Department of Chemistry, Lomonosov Moscow State University, 119991 Moscow, Russia

## Abstract

Recently, progress in IR sources, has led to the discovery that humans can infrared (IR) light. This is hypothesized due to two-photon absorption (TPA) events promoting the retina dim-light rod photoreceptor rhodopsin to the same excited state populated via one-photon absorption (OPA). Here, we combine quantum mechanics/molecular mechanics and extended multi-configuration quasi-degenerate perturbation theory calculations to simulate the TPA spectrum of bovine rhodopsin (Rh) as a model for the human photoreceptor. The results show that the TPA spectrum of Rh has an intense $S_0 \rightarrow S_1$ band but shows also $S_0 \rightarrow S_2$ and $S_0 \rightarrow S_3$ transitions whose intensities, relative to the $S_0 \rightarrow S_1$ band, is significantly increased when compared to the corresponding bands of the OPA spectrum. In conclusion, we show that IR light in the 950 nm region can be perceived by rod photoreceptors supporting the two-photon origin of the IR perception. We also found that the same photoreceptor can perceive red (*i.e.* close to 680 nm) light provided that TPA induces population of $S_2$.

## Graphical Abstract

**Corresponding Author** ioffe@thermo.chem.msu.ru and molivuc@bgsu.edu.

Author Contributions

The manuscript was written through contributions of all authors. All authors have given approval to the final version of the manuscript.

ASSOCIATED CONTENT

**Supporting Information**. Computational details for methodology, Charge distribution on the rPSB11 chromophore, further assessment on the accuracy of the QM/MM models, TPA spectra of reference molecules, OPA and TPA properties of rPSB11 in vacuum, Energies, BLA, dihedrals and HOOP profiles along the FC trajectories are provided in supporting information. This material is available free of charge via the Internet at http://pubs.acs.org (file type, i.e., DOC)

The authors declare no competing financial interest.

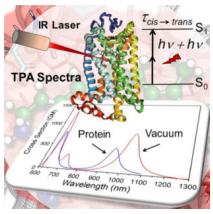


**Keywords**

Bovine Rhodopsin; Two Photon Absorption (TPA) Spectroscopy; Human Photoreceptor; Infrared (IR) Vision; Multi-State Multi-Configurational Second Order Perturbation (MS-MC-PT2) Theory

The vertebrate dim-light (scotopic) photoreceptor rhodopsin belongs to a large group of proteins forming the so-called G protein-coupled receptor (GPCR) family. More specifically, rhodopsin features the common hollow α-helical transmembrane structure of GCPR, but hosts an 11-*cis*-retinal chromophore (rPSB11) antagonist covalently connected to the protein via a protonated Schiff base linkage.[1–2] (see Scheme 1). The light-induced (*i.e.* photochemical) isomerization of the rPSB11 chromophore to its all-*trans* isomer (rPSBAT), is the first step of the so called rhodopsin photocycle ultimately leading to the production of the protein biologically active Meta-II state.[3]

For a long time, it has been thought that humans cannot perceive infrared (IR) radiation. However, in the 1970s it was discovered that the human retina perceives IR light in the 800–1355 nm range.[4–5] Second harmonic generation[6] in the eye, fluorescence and two-photon absorption (TPA)[7] were suggested as IR perception mechanisms. Several electrophysiological studies with lower vertebrate photoreceptors revealed a nonlinear optical processes leading to rhodopsin activation.[8–9] Although these studies imply that human visual perception might not be limited to the visible part of the electromagnetic spectrum, they did not explain how IR perception is allowed at the molecular level. Thus, their implications for photoreceptor activation, including human photoreceptors, has remained unidentified.

In 2014, Palczewski and coworkers[10] provided evidence that humans can detect IR light at wavelengths around 950–1000 nm and that this is perceived as visible light. The study indicates that IR irradiation causes the photoisomerization of the rPSB11 chromophore suggesting that IR laser beams could be used to scan the retina and detect eye problems in their early stages—before they become insurmountable, where the using of visible-wavelength lasers might damage the retina.

The present paper is focused on the possibility of computing, rather than measuring, the TPA spectra of rhodopsins using quantum chemistry. To this aim, a theoretical exploration of the TPA properties of Rh using a quantum mechanics/molecular mechanics (QM/MM) model based on multi-state multi-configurational second order perturbation (MS-MC-PT2) level of QM theory, is carried out. To do so we focus on the structurally resolved bovine rhodopsin (Rh)[1] dim-light photoreceptor whose amino acid sequence and wavelength of absorption

maximum ($\lambda_{max}$) are very close to those of human rhodopsin (93% identity and 498[11–12] vs. 496[13–14] nm respectively).

More specifically:

- **i.** We construct ten isolated QM/MM models of Rh based on a previously reported Automatic Rhodopsin Modelling (ARM) protocol[15–16] (see section S1 in the supporting information (SI), for computational details) and the XMCQDPT2 (*i.e.* extended multi-configuration quasi-degenerate perturbation theory) implementation of the MS-MC-PT2 theory and use it to determine the $\lambda_{max}$ and intensity (oscillator strength) of the OPA spectra. To assess the model accuracy, we compare the computed and experimental OPA features of Rh.
- **ii.** By focusing on two previously investigated molecules, *trans*-stilbene and a related stilbenoid,[17–19] we evaluate the reliability of XMCQDPT2 for the simulation of TPA spectra.
- **iii.** Finally, by using the constructed QM/MM model we compute the Rh TPA spectra and compare it with the available experimental data. The possible photochemical response of the TPA transition is then qualitatively evaluated using semi-classical trajectories.

## OPA properties of the XMCQDPT2/cc-pVTZ//CASSCF/6–31G(d)/AMBER QM/MM model of Rh.

The absorption spectrum of Rh shows three peaks in UV-Vis region.[20] The two principal peaks are located at 498[11] and 280[20–21] nm (57.4 and 102.1 kcal/mol, respectively). The long-wavelength peak is attributed to the $S_0 \rightarrow S_1$ transition[22] and short-wavelength intense peak attributed to aromatic amino acids.[20] However, the latter peak is also presents in the spectra of rPSB11 in 1,2-dichloroethane solvent[21] with lower intensity. The band at 498 nm corresponds to the lowest $\pi$-$\pi^*$ transition of the chromophore. There is a weaker peak at 340[12, 20, 23–24] nm (84.1 kcal/mol) assigned to the $S_0 \rightarrow S_2$ transition[22] which is only seen in rPSB11.[20]

In Table 1 we report the calculated average vertical excitation energies $\langle \Delta E_{S1-S0} \rangle$, $\langle \Delta E_{S2-S0} \rangle$ and $\langle \Delta E_{S3-S0} \rangle$ computed using the constructed 8-root state average XMCQDPT2/cc-pVTZ//CASSCF/6–31G(d)/AMBER Rh models (the right side of the "//" indicate the level employed for geometry optimization and the left side that used for the energy and property calculations) and compare them to the experimental values obtained by converting wavelengths into vertical excitation energy values. Such excitations involve the ground state ($S_0$) and the first three singlet excited states (*i.e.* $S_1$, $S_2$ and $S_3$).

The results show that the $\langle \Delta E_{S1-S0} \rangle$ value is 60.1±0.5 kcal/mol ($\lambda_{max}$ = 475±4 nm) differs from the experimental value for less than 3.0 kcal/mol. After looking at the distribution of the positive charge along the chromophore backbone (see Scheme S1 and Table S2 in the SI) in $S_0$ and $S_1$, we see that the positive charge, initially located on the $-N=C_{15}-$ moiety, moves forward towards the β-ionone ring and conclude that $S_1$ has character in agreement with

previous studies.[22, 25–26] The $\langle \Delta E_{S2-S0} \rangle$ value is 84.3±0.4 ($\lambda_{max}$ = 339±2 nm) that differs from the experimental data of only 0.2 kcal/mol. Such kind of differences are also displayed by the corresponding values of the 10 uncorrelated QM/MM models (see Section S1 and Table S3 in the SI), which present errors in the 2.3 to 3.6 kcal/mol and 0.0 to 1.0 kcal/mol range, respectively. Notice that for $\Delta E_{S1-S0}$ these errors are close to the ca. 3.0 kcal/mol blue-shifted error previously documented for ARM generated QM/MM rhodopsin models.[15] Further assessment of the accuracy of the XMCQDPT2 method, the effect of basis set and variation in the number of contributing roots in the state averaging have been documented in section S4 of the SI. It is also worth to mention that a comprehensive investigation on the $S_0 \rightarrow S_3$ transition, and the effect of the protein environment on the $S_0 \rightarrow S_2$ and $S_0 \rightarrow S_3$ transitions have been reported in section S5 of the SI.

## TPA properties of trans-stilbene and a D-π-A stilbenoid.

The gas-phase *trans*-stilbene (see Scheme S2A in the SI) and its acceptor–π–donor (A–π–D) derivative 4-dimethylamino-4'-nitrostilbene (hereafter referred to as ACCD. See Scheme S2B in the SI) chromophores were used as benchmarks to validate the protocol for TPA spectra simulation. We selected ACCD because it features a non-centrosymmetric π-conjugation similar to rPSB11. The TPA cross section is related to the imaginary part of the second hyperpolarizability. Hence, our protocol is based on the Sum-Over-State (SOS) approach and accordingly, the equations "F1" and "D2" in Fortrie *et al.* [27] have been used to calculate the TPA line-shape as a function of the frequency ω, *i.e.* the excitation wavelength. Here, the SOS was approximated using eleven intermediate electronic states (12-root single point calculation, based on previous computations on conjugated chromophores of similar size,[28] see section S1 in the SI). In our protocol, two absorbed photons in TPA are degenerate and therefore, the calculated $\lambda_{max,\ TPA}$ and $\sigma_{TPA}$ values for *trans*-stilbene (see Figure S4A for the simulated spectra) can be defined as the values corresponding to the maximum of its TPA spectra as in previous studies[17–19, 29] (see Table 2). All calculated data reveal that while the obtained gas-phase $\lambda_{max,TPA}$ values match the experimental value measured in solution (toluene[17] and chloroform[29]) reasonably well, the calculated $\sigma_{TPA}$ by different methods, displays a substantial discrepancy (for more discussion see section S1 of the SI) which potentially may arise from the prediction of the transition dipole moments by different computational methods. In fact, comparing with experimental values, our computed TPA properties ($\lambda_{max,TPA}$ = 480 nm and σTPA= 32 GM) are in good agreement with the values reported by Wergifosse et. al,[29] ($\lambda_{max,TPA}$ = 486 nm and σTPA= 32 GM) rather than the values reported by Brédas et. al,[17] ($\lambda_{max,TPA}$ = 514 nm, and $\sigma_{TPA}$=12 GM). Furthermore, comparing to those computed with other methods,[18–19,29] XMCQDPT2 calculations shows the best agreement with the experimental data reported by Wergifosse et. al.[29]

The TPA spectra of *trans*-stilbene (see Figure S4A) show a peak centered at the $\lambda_{max,TPA}$ = 480 nm corresponds to the $S_0 \rightarrow S_4$ transition. According to our calculations, appreciable transition dipole moments from $S_0$ are found only for $S_0 \rightarrow S_1$ (5.7 Debye) and $S_0 \rightarrow S_3$ (5.0 Debye) pointing to this fact that the most intense TPA transition of $S_0 \rightarrow S_4$ could happen via the intermediate states $S_1$ or $S_3$ (*i.e.* $S_0 \rightarrow S_1 \rightarrow S_4$ or $S_0 \rightarrow S_3 \rightarrow S_4$, respectively). Inspection of the computed quantities and comparison with the results of the Brédas et. al,[17]

corroborate the dominant contribution of the $S_0 \rightarrow S_1 \rightarrow S_4$ transition in TPA spectra with the transition dipole moments of 5.7 Debye for $S_0 \rightarrow S_1$ and 2.5 Debye for $S_1 \rightarrow S_4$, analogous to that reported in Brédas et. al[17] (*i.e.* 7.1 and 3.1 Debye for $S_0 \rightarrow S_1$ and $S_1 \rightarrow S_4$, respectively). In contrast, TDDFT prediction by Nayyar et. al [18] overestimates the $S_1 \rightarrow S_4$ transition dipole moment by a factor of ~2.6 (8.2 Debye). This leads to the overestimation of the $\sigma_{TPA}$ by a factor of ~5 (note that their reported $\sigma_{TPA}$ values are in the order of hundred). In conclusion, our gas-phase *trans*-stilbene study indicates that XMCQDPT2 predicts $\sigma_{TPA}$ in good agreement with experimental data due to the reasonable values obtained for the transition energies and transition dipole moments.

To understand the effect of molecular geometry on the TPA properties of *trans*-stilbene, the spectra of the MP2/cc-pVTZ optimized structure[28] was calculated (Figure S5). The result shows a maximum at 486 nm with the $\sigma_{TPA}$ of 29 GM, and hence, indicates a small effect of the geometry on the transition energies, dipole moments and, consequently, TPA properties of *trans*-stilbene. The geometry of ACCD was then optimized at the MP2/ccpVTZ and the gas-phase TPA spectra of ACCD was calculated using the same procedure used for *trans*-stilbene due to the complexity of considering the solvent effect. The corresponding TPA spectra are shown in Figure S4B. One of the spectral characteristics of such D-π-A molecules is the absence of symmetry rules governing optical absorption properties of centrosymmetric molecules and therefore, any excited state becomes both one- and two-photon allowed. Furthermore, these D-π-A molecules (also known as push-pull molecules) show, in general, larger TPA cross section with respect to *trans*-stilbene.

The calculated OPA vertical excitation energy ($\lambda_{max,OPA}$ = 332 nm, see Table 2) of ACCD, corresponding to the $S_0 \rightarrow S_1$ transition, is in good agreement with the OPA gas-phase measurements (*i.e.* in a supersonic jet expansion.[37] See Table 2, value in parentheses). This indicates the reliability of our protocol in predicting the OPA properties of D-π-A chromophores. However, this value is far from that of experimental OPA spectra ($\lambda_{max,OPA}$ = 452 nm) in DMSO solvent [30, 32] pointing to a solvatochromic effect whose simulation would require an effort going beyond the scope of the present work. Such effect is expected to cause substantial structural and property (such as absorption spectra, hyperpolarizabilities and TPA cross sections) variation. In fact, DFT-based QM/MM calculations [31, 33] have showed that, in contrast with the case of *trans*-stilbene in an apolar solvent, a polar solvent (such as DMASO and water) induced geometrical changes are important to accurately predict the OPA and TPA spectra of ACCD. Thus, in principle, when comparing our calculated results to the experiment, it would be important to consider the effects of the medium.[31, 33] However, we noticed that when comparing the changes in the experimental $\lambda max, TPA$ and $\sigma_{TPA}$ values going from *trans*-stilbene to ACCD (486 to 909 nm and 32 to 191 GM, respectively), our XMCQDPT2-based methodology provide the same trend (480 to 664 nm and 32 to 141 GM, respectively). We take this as supportive for the protocol qualitative validity for TPA spectra simulation. It is also worth mentioning that our calculated $\sigma_{TPA}$ value for ACCD is comparable with the value obtained by QM/MM studies probing the solvatochromic effect (see Table 2).[31, 33]

## TPA properties of Rh.

The predicted $\sigma_{TPA}$ and $\lambda_{max,TPA}$ values from 10 uncorrelated *XMCQDPT2/cc-pVTZ//CASSCF/6–31G(d)/AMBER* models of Rh, have allowed to simulate the TPA band presented in Figure 1. The simulated spectra reflect the blue shift of the OPA spectra of Rh with respect to the gas-phase chromophore[38–40] (Figure S6). The data predict an average TPA cross section of 472 GM at $\lambda_{max,TPA}$ = 950 nm, for the TPA corresponding to the $S_0 \rightarrow S_1$ transition. The calculated $\sigma_{TPA}$ value is comparable with the relatively high value reported for the close system channelrhodopsin 2 (ChR2) which is ~ 260 GM at 920 nm.[36] The predicted $\lambda_{max,TPA}$ value matches the value predicted in a previous theoretical study, reporting an absorption between 950–1150 nm with a ~1000 nm maximum[10] and demonstrating the consistency of such value with experimental electrophysiology data on the sensitivity to IR light of rods and, possibly, cones photoreceptor cells. However, our $\sigma_{TPA}$ value is different from that computed in the same study. A fact that may be attributed to the use of TDDFT to compute the transition dipole moments or to the choice of macroscopic conversion pre-factor. Additionally, analyzing the important orbitals involved in TPA transitions (see section S8 in the SI for details), in consistent with the charge distribution on the rPSB11 chromophore (Table S2 in the SI) corroborates the charge transfer character of $S_0 \rightarrow S_1$ transition induced by TPA. Accordingly, considering the incorrect description of charge-transfer excitations as one of the hallmark failures of TDDFT,[41] shows the superiority of our protocol for reliable prediction of the TPA properties of Rh.

As mentioned above, the computed $\lambda_{max,TPA}$ (~1000 nm) corresponds to the energy gap of 60.2 kcal/mol results in electronic excitation of the rPSB11 chromophore to its $S_1$ state. The $S_0 \rightarrow S_1$ vertical excitation corresponds to a $\pi \rightarrow \pi^*$ transition which is also responsible for the rapid 11-*cis* to all-*trans* photo-isomerization of rPSB11.[42] Therefore, as concluded in Palczewska et. al,[10] our calculations is consistent with an effective Rh IR light perception and with the hypothesis that OPA and TPA result in the same photoisomerization process, producing rPSBAT and therefore activating the Rh photocycle and, in turn, visual perception.[10] This appears to be a straightforward conclusion when considering the computational and experimental evidence in favor of a barrierless nature of the $S_1$ double-bond isomerization path and the results of semi-classical trajectory simulations as well as time-resolved absorption spectroscopy experiments.[22, 43]

OPA and TPA calculations of our Rh QM/MM model demonstrate that while the second excitation ($S_0 \rightarrow S_2$) of the Rh is weak in the OPA spectra (see the oscillator strengths in Table 1), it is somehow more intense in TPA (Figure 1). As also evident from Table 1, these observations match well with the reported OPA[12, 20, 23–24] experimental spectra which shows a weak peak at the $\beta$ band of the Rh corresponding to the $S_0 \rightarrow S_2$ transition. In our study, the calculated average $\lambda_{max,TPA}$ of the Rh models, related to the $S_0 \rightarrow S_2$ transition, is located at 678 ($2 \times \lambda_{max,OPA}$ = 339) nm with the average cross section of 231 GM.

We compared our Rh computed TPA spectra with the corresponding experimental spectra reported by Birge et al.[35] In such study, the $S_1$ and $S_2$ states appear close to each other being assigned to a ~490 nm (as appeared in the OPA experiment) and ~440 nm (appeared in the TPA experiment) values, respectively.[35] Based on their experiment, the $\lambda_{max,TPA}$ is 909 nm

(11000 cmwhich is far from our predictions for the $\lambda_{max,TPA}$ of $S_0 \rightarrow S_2$ but matches well with the $\lambda_{max,TPA}$ of $S_0 \rightarrow S_1$. Furthermore, previously experimental studies showed a low-intensity band at 340 nm which can be assigned to the $S_0 \rightarrow S_2$ transition.[12, 20] This assignment is supported by gas-phase[40, 44] and our QM/MM calculations, which is observed well separated transitions to the $S_1$ and $S_2$ states, challenging the $S_2$ assignment by Birge et al.[35]

The calculated average $\lambda_{max,TPA}$ of our Rh models related to the $S_0 \rightarrow S_3$ transition, is located at 644 ($2 \times \lambda_{max,OPA}$ = 322) nm and shows an average $\sigma_{TPA}$ of 771 GM. Similar to the $S_0 \rightarrow S_2$ transition, the $S_0 \rightarrow S_3$ OPA transition is weak (*i.e.* it has a small oscillator strength) but, obviously, predicted to be strongly allowed in TPA. Furthermore, while both $S_0 \rightarrow S_2$ and $S_0 \rightarrow S_3$ transitions are predicted to have the same intensity in OPA (*i.e.* same oscillator strength), the later has a higher $s_{TPA}$ (771 GM vs. 231 GM). This could be explained in terms of dipole and transition dipole moments used in the Sum-Over-State (SOS) approach (see section S1, equation 2 in the SI). After looking at the transition dipole moments (see section S8, SI), it was found that the most important contributions to the $S_0 \rightarrow S_2$ and $S_0 \rightarrow S_3$ transitions in the TPA spectrum of Rh are $S_0 \rightarrow S_1 \rightarrow S_2$ and $S_0 \rightarrow S_1 \rightarrow S_3$, respectively. The related transition dipole moments are 9.4, 5.0, and 7.5 Debye for $S_0 \rightarrow S_1$, $S_1 \rightarrow S_2$ and $S_1 \rightarrow S_3$ transitions, respectively. The higher transition dipole moment of $S_1 \rightarrow S_3$ by the factor of ~1.5 with respect to the $S_1 \rightarrow S_2$ leads to the larger $\sigma_{TPA}$ of $S_0 \rightarrow S_3$. Looking at the transition diploe moments provides the explanation for different intensity of $S_0 \rightarrow S_2$ and $S_0 \rightarrow S_3$ transitions in OPA and TPA. This value for both OPA transitions corresponds to 3.8 Debye (note to the same oscillator strength), which is much smaller than the transition dipole moments responsible for the two-photon transitions (9.4, 5.0, and 7.5 Debye for $S_0 \rightarrow S_1$, $S_1 \rightarrow S_2$ and $S_1 \rightarrow S_3$ transitions, respectively). This also has been justified on the bases of molecular orbital excitations in the section S8 of SI.

The dynamics triggered by the population of the $S_1$, $S_2$ and $S_3$ potential energy surfaces has been investigated by computing the corresponding FC trajectories at the CASSCF/6–31G(d)/AMBER level of theory (see section S1 in the SI, for computational details) which are surface-hop trajectories starting from the $S_0$ equilibrium structure of our QM/MM representative model (*i.e.* model-6) with zero initial velocities. The analysis of the geometrical progression along the CASSCF-driven FC trajectories is provided in the SI (see Figure S8). In order to qualitatively account for the effect of dynamic electron correlation and to be consistent with the above spectral analysis, the energy profiles are also recomputed using the CASPT2//CASSCF/6–31G(d)/AMBER level of theory (Figure 2). As shown in the Figure 2, the shape of the CASPT2 and CASSCF energy profiles for the excited state progression of Rh are similar. However, as expected, the CASPT2 energies are red-shifted due to the inclusion of dynamic electron correlation. FC trajectories provide an approximate description of the motion of the center of the excited state population and, in the present context, are used to provide qualitative evidence that the reactive $S_1$ state gets populated after TPA to the $S_2$ and $S_3$ states. Accordingly, we begin by showing that, with the constructed QM/MM model, the FC trajectory of Rh computed at the two-root state-average CASSCF/6–31G(d)/AMBER level and corrected by three-root state-average CASPT2 level, starting on $S_1$, reaches the reactive $S_1/S_0$ conical intersection on a ca. 100 fs timescale (Figure 2A), CI1 and CI1-like points in CASSCF and CASPT2 profiles, respectively) as

previously documented with other models for the OPA process.[26, 45] This is taken as an evidence that the rPSB11 chromophore in the adopted Rh model undergoes isomerization and that the primary photocycle intermediate bathorhodopsin is produced upon decay and relaxation on the $S_0$ potential energy surface upon IR irradiation. In order to demonstrate that the reactivity is maintained also when populating the $S_2$ state, we computed the FC trajectory at the same level of theory but employing three-root state-average orbitals in both CASSCF and CASPT2 calculations and starting on $S_2$ (see Figure 2B). The results indicate that $S_1$ is populated after ~15 fs (CI2 and CI2-like in CASSCF and CASPT2 profiles, respectively) upon decay from $S_2$ to $S_1$. To provide evidence for a reactive populated region of $S_1$, we stop the trajectory 10 fs after $S_1$ population and restart it from the same geometry and velocities and level of theory but with the more accurate two-root state average CASSCF wavefunction. The $S_1$ population reaches the reactive $S_1/S_0$ conical intersection on a ca. 100 fs timescale (Figure 2B), CI1 and CI1-like points in CASSCF and CASPT2 profiles, respectively).

Finally, in order to assess the reactivity of the TPA excitation to $S_3$ we compute a FC trajectory at the three-root state-average level (from the second to the fourth root) starting from $S_3$. We show that the $S_3$ doesn't decay after ~110 fs (see Figure 2C). Accordingly, in contrast with TPA excitation to $S_2$ and $S_1$, we see that excitation to $S_3$ does not yield a fast decay to the $S_1$ state and hence, a fast $S_1$-like reactivity (the lack of progress along the isomerization coordinate is documented in the SI, Figure S8C). A much longer dynamics would be required to establish if this state is bounded (*i.e.* emissive) or if simply reacts on a much longer timescale.

We have simulated the TPA spectra of the dim-light visual receptor Rh, using a set of QM/MM models constructed via a semi-automatic protocol. Such models allow to use MS-MC-PT2 theory to consistently calculate OPA and TPA spectral properties, ultimately leading to an effective XMCQDPT2/cc-pVTZ//CASSCF/6–31G(d)/AMBER protocol, then validated by comparing computed and experimental quantities for *trans*-stilbene in its $C_2$ non-centrosymmetric equilibrium geometry and its polar D-π-A derivative ACCD. The comparison shows that the protocol yields transition dipole moments and transition energies and, hence, $\sigma_{TPA}$ values comparable with experimental data.

The calculated energies and transition dipole moments of the 10 Rh models, allowed to predict an average $\sigma_{TPA}$ of 472 GM at $\lambda_{max,TPA}$ = 950 nm, for the $S_0 \rightarrow S_1$ transition. This fully support the hypothesis that a cattle eye and, most likely, the human eye can detect IR light which is then perceived as visible light. However, the computed $\sigma_{TPA}$ value appears to be different from that reported in Palczewska et. al.,[10] a fact that may be attributed to the use of TDDFT to calculate the transition dipole moments or to the choice of the macroscopic conversion pre-factor.

While the $S_0 \rightarrow S_2$ OPA transition of Rh is very weak, its intensity is increased in the TPA spectrum. More specifically, the computed average $\sigma_{TPA}$ is 231 GM at $\lambda_{max,TPA}$ = 678 nm. Such $S_0 \rightarrow S_2$ $\lambda_{max,TPA}$ value appears quite different with respect to the experimentally derived value reported by Birge et al. possibly due to the wrong assignment of the $S_2$ state as shown in this paper and also pointed out by Andersen et al.[40, 44] in the study of the gas-

phase rPSB chromophore. On the other hand, while a possible contribution to the assignment of intermolecular charge transfer states (e.g. between the retinal chromophore and a conjugated cavity side chain) cannot be excluded, our QM/MM model is unable to deal with such event that will have to be investigated in future work by trying to extend the model QM subsystem.

The capability of two-photon excitation microscopy (TPM) to detect retinal disfunctions has been successfully confirmed in vivo by Palczewska et. al.,[46–47] thus showing the potential of two-photon imaging for monitoring early retinoid changes. Due to the possibility of increasing the intrinsic fluorescence of the retinal chromophore via suitable mutations or by using microbial rhodopsins, large cross section values in our calculations asserted that rPSB11 could be turned into a fluorescent probe[48] for two-photon microscopy for *in vivo* imaging and monitoring in the red and infrared light regime with the least light-induced damage of living cells. Furthermore, in agreement with the previous experimental studies [49–50] which approve the applicability of near-infrared (NIR) laser (via TPA) to investigate the activation of channelrhodopsin, our model and predicted TPA properties are promising for the computational investigation of rhodopsins (e.g. ChR2) useful in optogenetics.

In conclusion, our calculations show that ca. 950 nm light can be perceived by the green-blue light absorbing Rh photoreceptor at the TPA level, thus supporting the two-photon origin of the IR perception. We also provide evidence, by using semi-classical trajectory calculations, that via TPA Rh can also perceive (see) red light (*i.e.* close to 678 nm), as population of $S_2$ ultimately leads to chromophore isomerization through a conventional $S_1$ path. However, TPA population of $S_3$ may not lead to chromophore isomerization with the same speed of $S_2$ and $S_1$ population. Therefore, it is likely that TPA-based perception of a wavelength of 643 nm (ca. orange light) cannot be detected with the same type of mechanism or occur through a significantly slower reaction channel.

## Supplementary Material

Refer to Web version on PubMed Central for supplementary material.

## ACKNOWLEDGMENT

The research has been supported by the following grants NSF CHE-CLP-1710191 and NIH GM126627 01. MO is grateful for a USIAS 2015 grant. S.G., X.Y. and M.O. thank the Ohio Suprcomputer Center for awarded computational resources. The research was carried out partly using the equipment of the shared research facilities of HPC computing resources at Lomonosov Moscow State University.

Funding Sources

NIH (National Institute of Health) grant number NIH GM126627 01

NSF (National Science Foundation) grant number NSF CHE-CLP-1710191

## ABBREVIATIONS

| | |
|---|---|
| **TPA** | Two Photon Absorption |
| **OPA** | One photon Absorption |

| | |
|---|---|
| **Rh** | Bovine Rhodopsin |
| **XMCQDPT2** | Extended Multi-Configuration Quasi-Degenerate Second Order Perturbation Theory |
| **QM/MM** | Quantum Mechanic/Molecular Mechanic |
| **rPSB11** | 11-*cis*-retinal chromophore |
| **ChR2** | Channelrhodopsin-2 |
| **DFT** | Density Functional Theory |
| **TDDFT** | Time Dependent Density Functional Theory |

## REFERENCES


1. Okada T; Sugihara M; Bondar A-N; Elstner M; Entel P; Buss V The retinal conformation and its environment in rhodopsin in light of a new 2.2 Å crystal structure. J. Mol. Biol. 2004, 342 (2), 571–583. [PubMed: 15327956]
2. Wald G The molecular basis of visual excitation. Nature. 1968, 219 (5156), 800. [PubMed: 4876934]
3. Palings I; Pardoen JA; Van den Berg E; Winkel C; Lugtenburg J; Mathies RA Assignment of fingerprint vibrations in the resonance Raman spectra of rhodopsin, isorhodopsin, and bathorhodopsin: implications for chromophore structure and environment. Biochemistry 1987, 26 (9), 2544–2556. [PubMed: 3607032]
4. Dmitriev VG; Emel'yanov V; Kashintsev M; Kulikov VV; Solov'ev A; Stel'makh M; Cherednichenko OB Nonlinear perception of infrared radiation in the 800–1355 nm range with human eye. Sov. J. Quantum Electron. 1979, 9 (4), 475.
5. Sliney DH; Wangemann RT; Franks JK; Wolbarsht ML Visual sensitivity of the eye to infrared laser radiation. J. Opt. Soc. Am. 1976, 66 (4), 339–341. [PubMed: 1262982]
6. Zaidi Q; Pokorny J Appearance of pulsed infrared light: second harmonic generation in the eye. Appl. Opt. 1988, 27 (6), 1064–1068. [PubMed: 20531520]
7. Denk W; Strickler JH; Webb WW Two-photon laser scanning fluorescence microscopy. Science. 1990, 248 (4951), 73–76. [PubMed: 2321027]
8. Gray-Keller M; Denk W; Shraiman B; Detwiler PB Longitudinal spread of second messenger signals in isolated rod outer segments of lizards. J. Physiol. 1999, 519 (3), 679–692. [PubMed: 10457083]
9. Euler T; Hausselt SE; Margolis DJ; Breuninger T; Castell X; Detwiler PB; Denk W Eyecup scope—optical recordings of light stimulus-evoked fluorescence signals in the retina. Pflugers. Arch. 2009, 457 (6), 1393–1414. [PubMed: 19023590]
10. Palczewska G; Vinberg F; Stremplewski P; Bircher MP; Salom D; Komar K; Zhang J; Cascella M; Wojtkowski M; Kefalov VJ Human infrared vision is triggered by two-photon chromophore isomerization. Proc. Natl. Acad. Sci. 2014, 111 (50), E5445–E5454. [PubMed: 25453064]
11. Morrow JM; Castiglione GM; Dungan SZ; Tang PL; Bhattacharyya N; Hauser FE; Chang BS An experimental comparison of human and bovine rhodopsin provides insight into the molecular basis of retinal disease. FEBS Lett. 2017, 591 (12), 1720–1731. [PubMed: 28369862]
12. Crouch R; Purvin V; Nakanishi K; Ebrey T Isorhodopsin II: artificial photosensitive pigment formed from 9, 13-dicis retinal. Proc. Natl. Acad. Sci. 1975, 72 (4), 1538–1542. [PubMed: 1055424]
13. Katai N; Kikuchi T; Shibuki H; Kuroiwa S; Arai J; Kurokawa T; Yoshimura N Caspaselike proteases activated in apoptotic photoreceptors of Royal College of Surgeons rats. Investig. Ophthalmol. Vis. Sci. 1999, 40 (8), 1802–1886. [PubMed: 10393051]

14. van Kuijk F; Lewis J; Buck P; Parker K; Kliger D Spectrophotometric quantitation of rhodopsin in the human retina. Investig. Ophthalmol. Vis. Sci. 1991, 32 (7), 1962–1967. [PubMed: 2055690]
15. Melaccio F; del Carmen Marín M; Valentini A; Montisci F; Rinaldi S; Cherubini M; Yang X; Kato Y; Stenrup M; Orozco-Gonzalez Y Toward automatic rhodopsin modeling as a tool for high-throughput computational photobiology. J. Chem. Theory Comput. 2016, 12 (12), 6020–6034. [PubMed: 27779842]
16. Pedraza-González L; De Vico L; Marín M. a. d. C.; Fanelli F; Olivucci M a-ARM: Automatic Rhodopsin Modeling with Chromophore Cavity Generation, Ionization State Selection, and External Counterion Placement. J. Chem. Theory Comput. 2019, 15 (5), 3134–3152. [PubMed: 30916955]
17. Albota M; Beljonne D; Brédas J-L; Ehrlich JE; Fu J-Y; Heikal AA; Hess SE; Kogej T; Levin MD; Marder SR Design of organic molecules with large two-photon absorption cross sections. Science. 1998, 281 (5383), 1653–1656. [PubMed: 9733507]
18. Nayyar IH; Masunov A m. E.; Tretiak, S. Comparison of TD-DFT methods for the calculation of two-photon absorption spectra of oligophenylvinylenes. J. Phys. Chem. C. 2013, 117 (35), 18170–18189.
19. Morel Y; Irimia A; Najechalski P; Kervella Y; Stephan O; Baldeck PL; Andraud C Two-photon absorption and optical power limiting of bifluorene molecule. J. Chem. Phys. 2001, 114 (12), 5391–5396.
20. Ebrey TG; Honig B Ultraviolet chromophore transitions in the rhodopsin spectrum. Proc. Natl. Acad. Sci. 1972, 69 (7), 1897–1899. [PubMed: 4505668]
21. Erickson JO; Blatz PE N-retinylidene-1-amino-2-propanol: a Schiff base analog for rhodopsin. Vision research 1968, 8 (10), 1367–1375. [PubMed: 5713206]
22. Frutos LM; Andruniów T; Santoro F; Ferré N; Olivucci M Tracking the excited-state time evolution of the visual pigment with multiconfigurational quantum chemistry. Proc. Natl. Acad. Sci. 2007, 104 (19), 7764–7769. [PubMed: 17470789]
23. Shichi H Biochemistry of visual pigments II. Phospholipid requirement and opsin conformation for regeneration of bovine rhodopsin. J. Biol. Chem. 1971, 246 (20), 6178–6182. [PubMed: 5127425]
24. Rafferty CN; Cassim JY; McConnell DG Circular dichroism, optical rotatory dispersion, and absorption studies on the conformation of bovine rhodopsin in situ and solubilized with detergent. Biophysics of structure and mechanism 1977, 2 (4), 277–320.
25. Cembran A; Bernardi F; Olivucci M; Garavelli M The retinal chromophore/chloride ion pair: Structure of the photoisomerization path and interplay of charge transfer and covalent states. Proc. Natl. Acad. Sci. 2005, 102 (18), 6255–6260. [PubMed: 15855270]
26. Manathunga M; Yang X; Orozco-Gonzalez Y; Olivucci M Impact of Electronic State Mixing on the Photoisomerization Time Scale of the Retinal Chromophore. J. Phys. Chem. Lett. 2017, 8 (20), 5222–5227. [PubMed: 28981285]
27. Fortrie R; Chermette H Two-photon absorption strength: A new tool for the quantification of two-photon absorption. J. Chem. Phys. 2006, 124 (20), 204104.
28. Ioffe I; Granovsky A Photoisomerization of stilbene: The detailed XMCQDPT2 treatment. J. Chem. Theory Comput. 2013, 9 (11), 4973–4990. [PubMed: 26583415]
29. De Wergifosse M; Houk AL; Krylov AI; Elles CG Two-photon absorption spectroscopy of trans-stilbene, cis-stilbene, and phenanthrene: Theory and experiment. J. Chem. Phys. 2017, 146 (14), 144305.
30. Antonov L; Kamada K; Ohta K; Kamounah FS A systematic femtosecond study on the two-photon absorbing D-π-A molecules–π-bridge nitrogen insertion and strength of the donor and acceptor groups. Phys. Chem. Chem. Phys. 2003, 5 (6), 1193–1197.
31. Murugan NA; Kongsted J; Rinkevicius Z; Aidas K; Mikkelsen KV; Ågren H Hybrid density functional theory/molecular mechanics calculations of two-photon absorption of dimethylamino nitro stilbene in solution. Phys. Chem. Chem. Phys. 2011, 13 (27), 12506–12516.
32. Wielgus M; Bartkowiak W; Samoc M Two-photon solvatochromism. I. Solvent effects on two-photon absorption cross section of 4-dimethylamino-4′-nitrostilbene (DANS). Chem. Phys. Lett. 2012, 554, 113–116.

33. Lu S-I Discrete Solvent Reaction Field Calculations for One-and Two-Photon Absorptions of Solution-Phase Dimethylamino Nitro Stilbene Molecule. J. Phys. Chem. A. 2019.
34. Ohta K; Antonov L; Yamada S; Kamada K Theoretical study of the two-photon absorption properties of several asymmetrically substituted stilbenoid molecules. J. Chem. Phys. 2007, 127 (8), 084504.
35. Birge RR; Murray LP; Pierce BM; Akita H; Balogh-Nair V; Findsen LA; Nakanishi K Two-photon spectroscopy of locked-11-cis-rhodopsin: evidence for a protonated Schiff base in a neutral protein binding site. Proc. Natl. Acad. Sci. 1985, 82 (12), 4117–4121. [PubMed: 2987964]
36. Rickgauer JP; Tank DW Two-photon excitation of channelrhodopsin-2 at saturation. Proc. Natl. Acad. Sci. 2009, pnas. 0907084106.
37. Rijkenberg R; Bebelaar D; Buma W; Hofstraat J Isolated building blocks of photonic materials: High-resolution spectroscopy of excited states of jet-cooled push-pull stilbenes. J. Phys. Chem. A. 2002, 106 (11), 2446–2456.
38. Sekharan S; Weingart O; Buss V Ground and excited states of retinal Schiff base chromophores by multiconfigurational perturbation theory. Biophys. J. 2006, 91 (1), L07–L09. [PubMed: 16648170]
39. Andersen LH; Nielsen IB; Kristensen MB; El Ghazaly MO; Haacke S; Nielsen MB; Petersen MÅ Absorption of Schiff-base retinal chromophores in vacuo. J. Am. Chem. Soc. 2005, 127 (35), 12347–12350.
40. Knudsen JL; Kluge A; Bochenkova AV; Kiefer HV; Andersen LH The UV-visible action-absorption spectrum of all-trans and 11-cis protonated Schiff base retinal in the gas phase. Phys. Chem. Chem. Phys. 2018, 20 (10), 7190–7194. [PubMed: 29480305]
41. Kümmel S Charge-Transfer Excitations: A Challenge for Time-Dependent Density Functional Theory That Has Been Met. Adv. Energy Mater. 2017, 7 (16), 1700440.
42. González-Luque R; Garavelli M; Bernardi F; Merchán M; Robb MA; Olivucci M Computational evidence in favor of a two-state, two-mode model of the retinal chromophore photoisomerization. Proc. Natl. Acad. Sci. 2000, 97 (17), 9379–9384. [PubMed: 10944211]
43. Schapiro I; Ryazantsev MN; Frutos LM; Ferré N; Lindh R; Olivucci M The ultrafast photoisomerizations of rhodopsin and bathorhodopsin are modulated by bond length alternation and HOOP driven electronic effects. J. Am. Chem. Soc. 2011, 133 (10), 3354–3364. [PubMed: 21341699]
44. Nielsen IB; Lammich L; Andersen LHS 1 and S 2 excited states of gas-phase Schiff-base retinal chromophores. Phys. Rev. Lett. 2006, 96 (1), 018304.
45. Luk HL; Melaccio F; Rinaldi S; Gozem S; Olivucci M Molecular bases for the selection of the chromophore of animal rhodopsins. Proc. Natl. Acad. Sci. 2015, 112 (50), 15297–15302.
46. Palczewska G; Golczak M; Williams DR; Hunter JJ; Palczewski K Endogenous fluorophores enable two-photon imaging of the primate eye. Investig. Ophthalmol. Vis. Sci. 2014, 55 (7), 4438–4447. [PubMed: 24970255]
47. Palczewska G; Dong Z; Golczak M; Hunter JJ; Williams DR; Alexander NS; Palczewski K Noninvasive two-photon microscopy imaging of mouse retina and retinal pigment epithelium through the pupil of the eye. Nat. Med. 2014, 20 (7), 785. [PubMed: 24952647]
48. Marín M. a. d. C.; Agathangelou D; Orozco-Gonzalez Y; Valentini A; Kato Y; Abe-Yoshizumi R; Kandori H; Choi A; Jung K-H; Haacke S Fluorescence enhancement of a microbial rhodopsin via electronic reprogramming. J. Am. Chem. Soc. 2018, 141 (1), 262–271. [PubMed: 30532962]
49. Mohanty SK; Reinscheid RK; Liu X; Okamura N; Krasieva TB; Berns MW In-depth activation of channelrhodopsin 2-sensitized excitable cells with high spatial resolution using two-photon excitation with a near-infrared laser microbeam. Biophys. J. 2008, 95 (8), 3916–3926. [PubMed: 18621808]
50. Andrasfalvy BK; Zemelman BV; Tang J; Vaziri A Two-photon single-cell optogenetic control of neuronal activity by sculpted light. Proc. Natl. Acad. Sci. 2010, 107 (26), 11981–11986.

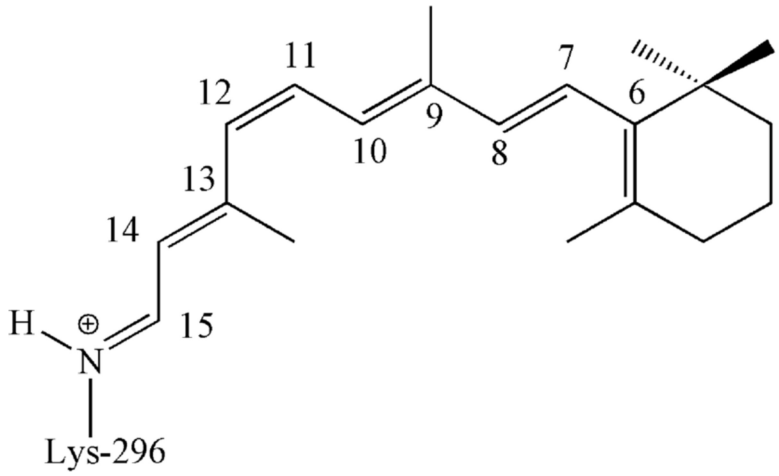


**Scheme 1.**
Chemical structure of rPSB11.

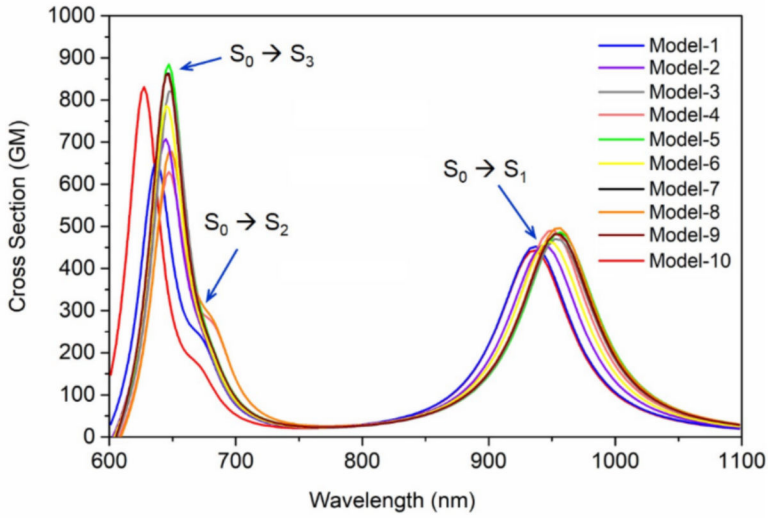


**Figure 1.**

TPA of Rh (rPSB11 embedded in the protein cavity) obtained from 10 QM/MM models at the XMCQDPT2 level of theory (XMCQDPT2/cc-pVTZ//CASSCF/6–31G(d)/AMBER models). The color code matches Figure S3.

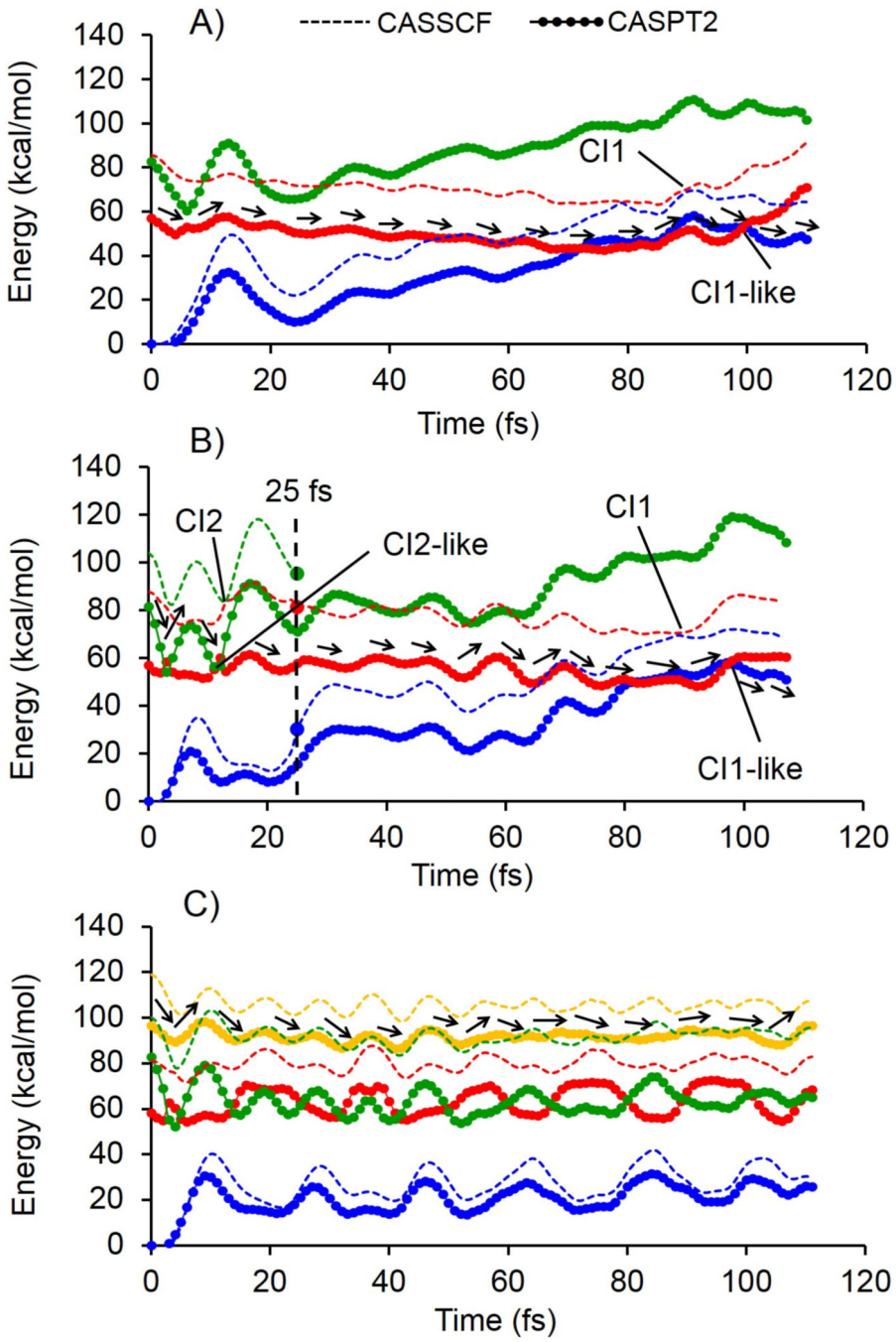


**Figure 2.**

Relative CASSCF (solid lines) and CASPT2 (solid line + circles) semi-classical energy profiles. A) Photoisomerization after population of the $S_1$ state. B) Photoisomerization after population of the $S_2$ state. The large full circles and dashed vertical line indicate the change in methodology from three-root to two-root state average in CASSCF energy profiles. C) Photoisomerization after population of the $S_3$ state. CI and CI-like points referred to

predicted conical intersection by CASSCF and CASPT2 level of theory, respectively. The stream of black arrows shows the reactive path at each trajectory.

**Table 1.**

Computed OPA spectroscopic properties of Rh with different approaches. Transition energies (vertical excitation energies) are given in kcal/mol (nm in parentheses).

| | ***Vertical (i.e. Franck-Condon) excitation*** | | | ***Oscillator Strength*** | | |
|---|---|---|---|---|---|---|
| **Method** | **$S_0 \rightarrow S_1$** | **$S_0 \rightarrow S_2$** | **$S_0 \rightarrow S_3$** | **$S_0 \rightarrow S_1$** | **$S_0 \rightarrow S_2$** | **$S_0 \rightarrow S_3$** |
| XMCQDPT2[1] | 60.1 (475 nm) | 84.3 (339 nm) | 88.8 (322 nm) | 0.88 | 0.20 | 0.20 |
| XMCQDPT2[2] | 60.2 (475 nm) | 84.3 (339 nm) | 88.5 (323 nm) | 0.87 | 0.20 | 0.21 |
| XMCQDPT2[3] | 60.3 (474 nm) | 84.3 (339 nm) | - | 0.87 | 0.18 | - |
| XMCQDPT2[4] | 63.7 (449 nm) | 86.4 (331 nm) | - | 0.84 | 0.26 | - |
| CASPT2 (IPEA=0)[5] | 57.5 (497 nm) | 83.6 (342 nm) | - | 0.60 | 0.38 | - |
| Experiment | 57.4 (498 nm) | 84.0 (340 nm) | | - | - | - |

[1] Average (10 models) 8-root SA with the cc-pVTZ basis set

[2] 8-root SA of the representative model (model-6) with the cc-pVTZ basis set

[3] 3-root SA of the representative model (model-6) with the cc-pVTZ basis set

[4] 3-root SA of the representative model (model-6) with the 6–31G(d) basis set

[5] 3-root SA with the 6–31G(d) basis set calculated with MOLCAS.

**Table. 2.**

Calculated and experimental OPA and TPA data for *trans*-stilbene, ACCD and Rh. $\lambda_{OPA}$ and $\lambda_{TPA}$ (nm) are, respectively, the lowest one-photon absorption wavelength and the two-photon resonance wavelength. $\sigma_{TPA}$ (GM; $10^{-50}$ $cm^4s$/photon-molecule) is the TPA cross section. For the choice of $\Gamma_{mn}$ value see page 11 in the SI.

| | | Theoretical Results | | | | Experimental Results | | | |
|---|---|---|---|---|---|---|---|---|---|
| | | $\lambda_{max,OPA}(nm)$ | $\lambda_{max,TPA}$ (nm) | $\sigma_{TPA}$ GM (a.u.) | $\Gamma_{mn}(eV)$ | | $\lambda_{max,OPA}$ (nm) | $\lambda_{max,TPA}$ (nm) | $\sigma_{TPA}$ GM |
| *trans*-stilbene | *this work* | 292 | 480 | 32(2033) | 0.2 | *ref (17)* | 297 | 514 | 12 |
| | *ref (17)*[a] | 278 | 466 | 27 | 0.1 | | | | |
| | *ref (19)*[b] | 267 | 469;425 | 280;54 | 0.25 | *ref (29)* | 302 | 486 | 32 |
| | *ref (18)*[c] | 471 | 397–514 | 117–129 | 0.2 | | | | |
| | *ref (29)*[d] | 273 | 432 | 43 | 0.2 | | | | |
| ACCD | *this work* | 332 | 664 | 141(9106) | 02 | *ref (30)* | 452 (335)[f] | 909 | 191 |
| | *ref (31)*[e] | 404–481 | - | 70–149 | 0.2–0.4 | | | | |
| | *ref (33)*[e] | 451 | - | 149 | - | *ref (32)* | 451 | 930 | 114 |
| | *ref (34)* | 279 | ~550 | ~30 | 0.248 | | | | |
| Rh | *this work* | 475 | 950 | 472 (30373) | 0.2 | *ref (10)* | 498[g] | 950–1050[h] 909[i] | 260[j] |
| | *ref (10)* | - | 1014 | 2.1 | - | | | | |

[a] Theoretical data from the INDO-MRD-CI method.

[b] Theoretical data from the CI-CNDO/S method.

[c] Theoretical data from the ATDA formalism.

[d] Theoretical data from the EOM-EE-CCSD method.

[e] Theoretical data from the TDDFT method.

[f] The value in parentheses is measured in the vacuum.

[g] The value is extracted from ref (11).

[h] The value is extracted from ref (10).

[i] The value is extracted from ref (35).

[j] The value is extracted from ref (36) for ChR2.